

# Situation-Aware Interactive MPC Switching for Autonomous Driving

Shuhao Qi <sup>\*,†</sup> Qiling Aori <sup>\*,†</sup> Luyao Zhang <sup>\*\*</sup> Mircea Lazar <sup>\*</sup>  
Sofie Haesaert <sup>\*</sup>

<sup>\*</sup> Eindhoven University of Technology, The Netherlands

<sup>\*\*</sup> Delft University of Technology, The Netherlands

**Abstract:** To enable autonomous driving in interactive traffic scenarios, various model predictive control (MPC) formulations have been proposed, each employing different interaction models. While higher-fidelity models enable more intelligent behavior, they incur increased computational cost. Since strong interactions are relatively infrequent in traffic, a practical strategy for balancing performance and computational overhead is to invoke an appropriate controller based on situational demands. To achieve this approach, we first conduct a comparative study to assess and hierarchize the interactive capabilities of different MPC formulations. Furthermore, we develop a neural network-based classifier to enable situation-aware switching among controllers with different levels of interactive capability. We demonstrate that this situation-aware switching can both substantially improve overall performance by activating the most advanced interactive MPC in rare but critical situations, and significantly reduce computational load by using a basic MPC in the majority of scenarios.

## 1. INTRODUCTION

Over the past decade, autonomous driving technology has advanced significantly and has recently been deployed in mass-produced vehicles as assistance to human drivers. However, autonomous driving algorithms still struggle in complex scenarios that require interaction with other road users, such as lane merging and roundabouts, which often necessitate human intervention. According to Wang et al. (2022), interaction occurs when the behaviors of two or more road users are mutually influenced by their potential competition for the same space in the near future. In such cases, the future behavior of other road users is inherently uncertain and multi-modal (Chen et al., 2022), and the behaviors of the involved traffic participants are mutually influential (Zanardi et al., 2021). In highly dynamic traffic environments, achieving safe and efficient interactive driving remains a significant challenge, particularly under limited computational resources.

Model predictive control (MPC) is a well-suited paradigm in autonomous driving thanks to its ability to handle constraints and uncertainty (Mesbah, 2018). Specifically, to ensure safety, *robust MPC* computes control inputs based on worst-case assumptions regarding the future behaviors of opponent vehicles (Zhou et al., 2022). Robust MPC often remains excessively conservative, as it considers improbable worst-case scenarios and neglects realistic interaction patterns between agents. To this end, *scenario trees* have been introduced to capture the multi-modal nature of opponent behaviors by enumerating a set of plausible future trajectories (Cesari et al., 2017; Muraleed-

haran et al., 2020). This approach is commonly referred to as *branch MPC* (Chen et al., 2022) and *scenario-based MPC* (Batkovic et al., 2021). The scenario tree often predict opponent vehicles independently of the ego vehicle’s behavior (Batkovic et al., 2021; Cesari et al., 2017; Muraleedharan et al., 2020), leading to non-reactive opponent behavior. This simplification leads to overly conservative ego policies, as potential cooperative responses from opponent agents are ignored. To overcome this limitation, recent works have integrated opponent reaction models into the planning process (Chen et al., 2022; Oliveira et al., 2023). In practice, each vehicle exhibits distinct driving styles and intentions, which can be characterized by latent parameters (Tian et al., 2021; Hu et al., 2024). While the aforementioned approaches represent significant advances, they generally rely on passive observation, waiting for other agents to reveal their intentions. To address this limitation, *active information-seeking behavior* has recently gained attention (Tian et al., 2021; Hu et al., 2024), wherein the ego vehicle actively probes opponent behavior and leverages their reactions to reduce uncertainty. This behavior reflects the dual-control effect (Knaup et al., 2024; Sadigh et al., 2018), in which control actions are designed to simultaneously optimize task performance and information gathering. Thus, this MPC formulation is referred to as *dual MPC* (Baltussen et al., 2025). In summary, existing methods improve interactive performance by incrementally incorporating realistic interaction modeling, including multi-modal prediction, opponent reactions, and active information-seeking behavior behavior.

However, MPC formulations with higher-fidelity interaction models often incur expensive computational costs. In practice, vehicles do not consistently engage in strong interactions with others. Therefore, it is essential to adaptively determine the appropriate level of interactive control based on the real-time situations. To this end, we first

<sup>†</sup> These authors contributed to this paper equally.

This work is supported by the European project SymAware under grant No. 101070802, the European project COVER under grant No. 101086228, and the Dutch NWO Veni project CODEC under grant No. 18244. (Corresponding author: s.qi@tue.nl)

conduct a systematic comparison on the interaction capabilities of various MPC formulations, each incorporating different levels of interaction modeling and exhibiting distinct behaviors in handling interactions. Building on these insights, we develop a neural network-based classifier to achieve situation-aware switching among interactive MPCs. This switching strategy significantly reduces computational burden while preserving the interactive performance and advanced behaviors of high-level controllers, including active information-seeking.

## 2. PROBLEM FORMULATION AND STATEMENT

In this paper, we focus on two-vehicle interactions for simplicity, but the framework readily extends to multi-vehicle scenarios. We say that two vehicles are in an interactive scenario if their predefined paths intersect. Fig. 1 shows an exemplary one-lane ramp merging scenario with vehicle-to-vehicle interaction (Knaup et al., 2024).

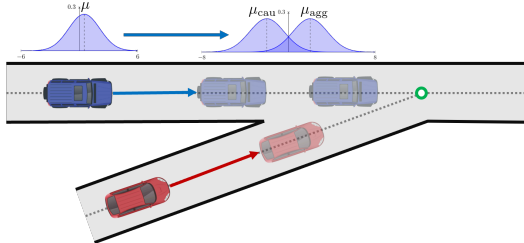


Fig. 1. One-lane ramp merging. The ego car (red) merges into the lane of the opponent car (blue). The opponent has different predictions under cautious ( $\mu_{cau}$ ) or aggressive behavior ( $\mu_{agg}$ ) when close to the ego.

The ego vehicle and opponent vehicle, denoted respectively with  $i \in \{e, o\}$ , both follow a predefined path given as

$$\mathcal{T}^i : S \rightarrow \mathbb{R}^2 \text{ with } S \subset \mathbb{R}. \quad (1)$$

Along these paths, we define the longitudinal behavior (Muraleedharan et al., 2020) based on the states  $x^i = [s^i, v^i]^\top \in \mathbb{R}^2$  for vehicles  $i \in \{e, o\}$ , where  $s^i \in S$  is the location on the path and  $v^i \in \mathbb{R}$  is the longitudinal speed. The longitudinal dynamics of each vehicle are modeled by

$$x_{t+1}^i = f(x_t^i, u_t^i) \quad (2)$$

where the input  $u_t^i \in \mathbb{R}$  is the longitudinal acceleration. We consider interactive scenarios in which the paths  $\mathcal{T}^e$  and  $\mathcal{T}^o$  intersect or overlap, that is,

$$\exists s_e, s_o : \|\mathcal{T}^e(s^e) - \mathcal{T}^o(s^o)\| < d_{safe}, \quad (3)$$

where  $d_{safe}$  denotes the safety distance between vehicles. Vehicles involved in such interactive scenarios are considered safe if they satisfy the following condition at all times:

$$\forall t : h(x_t^e, x_t^o) := \|p_t^e - p_t^o\| - d_{safe} \geq 0, \quad (4)$$

with the Cartesian position  $p_t^i = \mathcal{T}^i(s_t^i) \in \mathbb{R}^2$ .

### 2.1 Opponent behavior model

The control input of opponent vehicles  $u_t^o$  is generated by a behavior model designed to emulate realistic driver behavior. Following driver models in (Hu et al., 2024; Muraleedharan et al., 2020; Wang et al., 2019), we construct a parametric model that incorporates three key features: (i) uncertainty, (ii) responsiveness to other vehicles, and (iii) latent parameters. Accordingly, we define the behavior model using an i.i.d. Gaussian distribution:

$$u_t^o \sim \mathcal{N}(\mu_\theta(x_t^o, x_t^e), \sigma^2), \quad (5)$$

where the mean function  $\mu_\theta(x_t^o, x_t^e)$  depends on the states of both vehicles. The latent parameter vector  $\theta \in \Theta \subset \mathbb{R}^{n_\theta}$  is drawn from a finite set  $\Theta$  representing driver characteristics. The variance  $\sigma^2$  represents behavioral variability.

**Example:** To model the likely reactions (yielding or not yielding) of an opponent vehicle as the ego vehicle approaches, the mean  $\mu_\theta(x_t^o, x_t^e)$  is designed by the following piecewise function,

$$\mu_\theta(x_t^o, x_t^e) = \begin{cases} K(v^e + \theta \cdot \Delta v - v^o), & \|p_t^e - p_t^o\| \leq d_{int} \\ K(v^{o*} - v^o), & \text{otherwise} \end{cases} \quad (6)$$

where  $v^o$  and  $v^e$  are the velocities of the opponent and ego vehicles, respectively;  $v^{o*}$  is a desired cruising speed;  $\Delta v > 0$  is a constant speed adjustment;  $K$  is a control gain; and  $d_{int}$  is a distance threshold below which the opponent initiates a reactive behavior. The hidden parameter  $\theta \in \Theta$  is a scalar. For simplicity, we assume a binary set  $\Theta = \{\theta_{cau}, \theta_{agg}\}$ , with  $\theta_{cau} = -1$  representing cautious (yielding) behavior and  $\theta_{agg} = 1$  representing aggressive (non-yielding) behavior. As shown in Fig. 1, the opponent tracks  $v^{o*}$  when far from the ego, and switches to one of two reactive policies within the interaction distance of the ego car.

### 2.2 Problem statement

In interactive scenarios defined in Eq. (1) and (3), the control objective is to synthesize control inputs for the ego vehicle to track a desired speed  $v^{e*}$ , while ensuring safety in Eq. (4) with uncertain opponent vehicles whose behaviors follow the model in Eq. (5). As discussed in the introduction, a variety of interactive MPC formulations, including robust, branch, and dual MPC, differ in interaction capability and computational cost. To achieve advanced performance under limited on-board computational resources, we aim to develop a switching controller that adaptively selects controllers with appropriate levels of interactive capability based on situational demands.

## 3. INTERACTIVE MPC FORMULATIONS

In this section, we present five representative MPC formulations, each with a distinct level of interaction awareness. These levels are defined by whether the controllers incorporate multi-modal future, opponent reactions, and active information seeking, as summarized in Table 1.

### 3.1 Robust MPC

A common formulation of robust MPC is a min-max optimization problem (Scokaert and Mayne, 1998), where the controller minimizes the worst-case cost to ensure constraint satisfaction. In interactive driving (Zhou et al., 2022), this worst-case cost is evaluated by having the opponent maximize the objective within its admissible set:

$$\begin{aligned} & \min_{u_{0:H-1}^e} \max_{u_{0:H-1}^o} \sum_{k=0}^{H-1} \ell(x_k^e, u_k^e) + \ell_F(x_H^e) \\ \text{s.t. } & x_{k+1}^e = f(x_k^e, u_k^e), \quad x_{k+1}^o = f(x_k^o, u_k^o), \\ & h(x_{k+1}^e, x_{k+1}^o) \geq 0, \quad u_k^e \in \mathcal{U}^e, \quad u_k^o \in \mathcal{U}^o, \\ & x_0^e, x_0^o \text{ given,} \quad \forall k \in \{0, \dots, H-1\}, \end{aligned} \quad (7)$$

where  $h(\cdot)$  is defined in Eq. (4). The terms  $\ell(\cdot)$  and  $\ell_F(\cdot)$  denote the stage cost and terminal cost, respectively.

Table 1. Comparison of MPC formulations in the ramp merging scenario.

MPC formulation	Multi-modal future	Opponent reaction	Active probing	Related works
Robust	✗	✗	✗	Langson et al. (2004); Zhou et al. (2022)
Non-reactive branch	✓	✗	✗	Muraleedharan et al. (2020); Cesari et al. (2017)
Reactive branch	✓	✓	✗	Chen et al. (2022); Oliveira et al. (2023)
Explicit dual	✓	✓	✓	Sadigh et al. (2018); Baltussen et al. (2025)
Implicit dual	✓	✓	✓	Hu et al. (2024); Knaup et al. (2024)

Here, the stage cost  $\ell(x_k^e, u_k^e)$  penalizes deviation from a reference trajectory and the control effort, while the terminal cost  $\ell_F(x_H^e)$  penalizes the final deviation.

### 3.2 Branch MPC

Compared to robust MPC, a higher-level controller should plan over all plausible future interactions rather than optimizing for the worst case alone. To capture the multi-modal uncertainty inherent in interaction, a scenario tree is employed (Chen et al., 2022), with branches generated by sampling over the possible control inputs of the opponent vehicle. Each node corresponds to a realization of the system evolution, conditioned on a particular sampled opponent action. An example of the scenario tree is illustrated in Fig. 2. Let  $\mathbb{N} = \{n_0, n_1, \dots, n_{N-1}\}$  represent the set of nodes in a scenario tree, where  $N$  denotes the total number of tree nodes. The node  $n_0$  is designated as the root node and does not have a parent. Let  $\mathbb{L} \subseteq \mathbb{N}$  denote the set of *leaf nodes*, which do not have any child nodes. For each non-root node  $n \in \mathbb{N} \setminus \{n_0\}$ , the function  $\mathcal{P}(n)$  identifies its parent node. Conversely, for each non-leaf node  $n \in \mathbb{N} \setminus \mathbb{L}$ , the function  $\mathcal{C}(n)$  returns the set of its child nodes. Each non-root node is associated with a sampled opponent control input  $\hat{u}_n^o$ . Given  $\hat{u}_n^o$  and the ego control input at its parent node,  $u_{\mathcal{P}(n)}^e$ , the ego and opponent states at node  $n$ , denoted by  $x_n^e$  and  $x_n^o$ , are determined according to the system dynamics specified in Eq. (2). Since each ego control input  $u_n^e$  affects multiple child nodes,  $u_n^e$  is optimized to account for multiple sampled realizations at its child nodes. To mitigate node explosion while maintaining a long prediction horizon, tree generation is split into two phases (Hu et al., 2024): a branching horizon of length  $H_b$  with multiple samples, followed by a propagation horizon with a single nominal sample, as shown in Fig. 2.

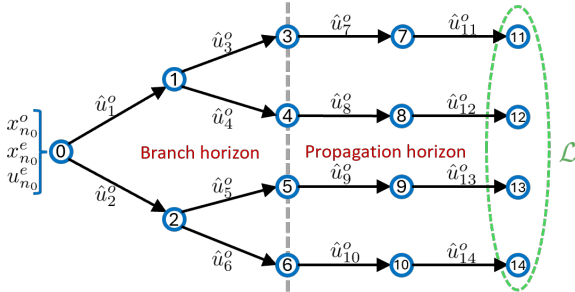


Fig. 2. A scenario tree with branching horizon  $H_b=2$ .

**Non-reactive branch MPC:** Following a common constant-speed assumption (Baltussen et al., 2025), we construct the scenario tree assuming the opponent maintains control inputs similar to its current behavior. As this assumption neglects potential reactions from opponent vehicles, it is referred to as *non-reactive branch MPC*.

Specifically, at each tree node  $n$ , the opponent's control input is modeled as  $\hat{u}_n^o = u_t^o + d_n$ , where  $u_t^o$  is the opponent's current control input and  $d_n \sim \mathcal{N}(0, \sigma^2)$  is an additive disturbance. The set  $\mathcal{D}_{\mathbb{N}} = \{d_n\}_{n \in \mathbb{N}}$  represents independent realizations of  $d_n \sim \mathcal{N}(0, \sigma^2)$ , one for each node in the tree. Let  $\mathbf{U}^e = \{u_n^e\}_{n \in \mathbb{N} \setminus \mathbb{L}}$  denote the set of ego control inputs at all non-leaf nodes, which are decision variables. Given this, the MPC minimizes the expected cost over the tree,

$$\begin{aligned} \min_{\mathbf{U}^e} \sum_{n \in \mathbb{N} \setminus \mathbb{L}} \ell(x_n^e, u_n^e) + \sum_{n \in \mathbb{L}} \ell_F(x_n^e) \\ \text{s.t. } x_n^e = f(x_{\mathcal{P}(n)}^e, u_{\mathcal{P}(n)}^e), \quad x_n^o = f(x_{\mathcal{P}(n)}^o, \hat{u}_n^o), \quad (8) \\ \hat{u}_n^o = u_{\mathcal{P}(n)}^o + d_n, \quad h(x_n^e, x_n^o) \geq 0, \\ u_{\mathcal{P}(n)}^e \in \mathcal{U}^e, \quad \forall n \in \mathbb{N} \setminus \{n_0\}, \end{aligned}$$

where the root node states  $x_{n_0}^e$  and  $x_{n_0}^o$  are initialized with the current actual states  $x_t^e$  and  $x_t^o$ , respectively. The stage cost  $\ell$  and terminal cost  $\ell_F$  are identical to those in Eq. (7).

**Reactive branch MPC:** To incorporate plausible opponent reactions, the scenario tree is constructed using the opponent's behavioral model defined in Eq. (5). The opponent's control input at node  $n$  is a function with an additive disturbance conditioned on its parent node:

$$\hat{u}_n^o = \mu_{\theta_n}(x_{\mathcal{P}(n)}^o, x_{\mathcal{P}(n)}^e) + d_n, \quad (9)$$

where  $d_n \sim \mathcal{N}(0, \sigma^2)$  and  $\theta_n \sim \text{Unif}(\Theta)$  are sampled offline at each node. Here,  $\text{Unif}(\cdot)$  denotes a uniform distribution over a set. Replacing the non-reactive sampling  $\hat{u}_n^o = u_t^o + d_n$  in Eq. (8) with Eq. (9) yields the *reactive branch MPC*.

### 3.3 Dual MPC

Similar to human drivers who can infer the driving styles and intentions of other vehicles through interaction, a higher-level controller should be capable of estimating the latent parameter  $\theta$ . Assuming the ego vehicle can perfectly observe the opponent's state, it has access to the information history at time  $t$ , denoted by  $\mathcal{I}_t = \{x_{0:t}^e, x_{0:t}^o\}$ . Given the finite set of latent parameters  $\Theta = \{\theta^1, \dots, \theta^W\}$  with  $|\Theta| = W$ , the belief state at time  $t$  is defined as the posterior distribution over the latent parameters given the interaction history  $\mathcal{I}_t$ :

$$b_t = \begin{bmatrix} b_t(\theta^1) \\ \vdots \\ b_t(\theta^W) \end{bmatrix} = \begin{bmatrix} \Pr(\theta = \theta^1 | \mathcal{I}_t) \\ \vdots \\ \Pr(\theta = \theta^W | \mathcal{I}_t) \end{bmatrix} \in \mathbb{R}^W, \quad (10)$$

where the belief vector satisfies the normalization constraint:  $\sum_{w=1}^W b_t(\theta^w) = 1$ . As the interaction progresses, the ego vehicle observes the opponent's next state  $x_{t+1}^o$  and estimates the opponent's input as  $\tilde{u}_t^o = \frac{v_{t+1}^o - v_t^o}{\Delta t}$ . Given the initial belief  $b_0$ , the belief over the latent parameter is updated via Bayesian inference:

$$b_t(\theta) = \frac{\rho_\theta(\tilde{u}_t^o | x_t^o, x_t^e) b_{t-1}(\theta)}{\sum_{\theta' \in \Theta} \rho_{\theta'}(\tilde{u}_t^o | x_t^o, x_t^e, \theta') b_{t-1}(\theta')}, \quad \forall \theta \in \Theta, \quad (11)$$

where  $\rho_\theta(\hat{u}_t^o | x_t^o, x_t^e) = \mathcal{N}(\hat{u}_t^o | \mu_\theta(x_t^o, x_t^e), \sigma^2)$  denotes the probability density of the policy distribution evaluated at  $\hat{u}_t^o$  specified in Eq. (5). This belief update is compactly expressed as  $b_t = \mathcal{B}(b_{t-1}, x_t^o, x_t^e)$  using the operator  $\mathcal{B}(\cdot)$ .

Since belief states quantify uncertainty and evolve with new information, incorporating belief updates into MPC formulations can induce a dual control effect. There are two main approaches to implementing dual MPC: (Mesbah, 2018; Arcari et al., 2020): the *explicit* approach introduces information gain into the objective function to encourage probing behavior (Sadigh et al., 2018), whereas the *implicit* approach incorporates belief evolution to couple estimation and planning (Hu et al., 2024).

**Explicit dual MPC:** Building upon the reactive branch MPC framework, the *explicit dual MPC* augments the objective function with an expected information gain associated with the current belief state:

$$\begin{aligned} \min_{\mathbf{U}^e} \sum_{n \in \mathbb{N} \setminus \mathbb{L}} \ell(x_n^e, u_n^e) + \sum_{n \in \mathbb{L}} \ell_F(x_n^e) + \sum_{n \in \mathbb{N}} E(b_t, x_n^e, x_n^o) \\ \text{s.t. } x_n^e = f(x_{\mathcal{P}(n)}^e, u_{\mathcal{P}(n)}^e), \quad x_n^o = f(x_{\mathcal{P}(n)}^o, \hat{u}_n^o), \quad (12) \\ \hat{u}_n^o = \mu_{\theta_n}(x_{\mathcal{P}(n)}^o, x_{\mathcal{P}(n)}^e) + d_n, \quad h(x_n^e, x_n^o) \geq 0, \\ u_{\mathcal{P}(n)}^e \in \mathcal{U}^e, \quad \forall n \in \mathbb{N}_t \setminus \{n_0\}, \end{aligned}$$

where the root node states  $x_{n_0}^e$  and  $x_{n_0}^o$  are initialized with the current real states  $x_t^e$  and  $x_t^o$ , respectively. The information gain  $E(b_t, x_n^e, x_n^o)$  is designed heuristically to elicit informative opponent reactions to facilitate the belief estimation (Sadigh et al., 2018; Baltussen et al., 2025).

**Example:** For the opponent model example given in Eq. (6), we define the gain function as

$$E(b_t, x_n^e, x_n^o) = C_e b_n(\theta_{\text{cau}}) b_n(\theta_{\text{agg}}) ((p_n^e - p_n^o)^2 - d_{\text{int}}^2),$$

where  $C_e$  is a constant weight, and the Cartesian positions  $p_n^e$  and  $p_n^o$  are computed according to Eq. (1). The term  $b_n(\theta_{\text{cau}}) b_n(\theta_{\text{agg}})$  serves as a measure of belief variance, which attains its maximum under a uniform belief distribution (i.e.,  $b_t = [0.5, 0.5]^\top$ ).

**Implicit dual MPC:** The implicit approach does not include an explicit information gain and instead integrates belief updates over the tree. Specifically, the belief state at node  $n \in \mathbb{N}$  is denoted by  $b_n$ . Each node's belief  $b_n$  is computed recursively from its parent's belief  $b_{\mathcal{P}(n)}$  using the state information at this node,  $(x_n^e, x_n^o)$ , with the belief update operator  $\mathcal{B}(\cdot)$ . The resulting implicit dual MPC is:

$$\begin{aligned} \min_{\mathbf{U}^e} \sum_{n \in \mathbb{N} \setminus \mathbb{L}} w_n \ell(x_n^e, u_n^e) + \sum_{n \in \mathbb{L}} w_n \ell_F(x_n^e) \\ \text{s.t. } x_n^e = f(x_{\mathcal{P}(n)}^e, u_{\mathcal{P}(n)}^e), \quad x_n^o = f(x_{\mathcal{P}(n)}^o, \hat{u}_n^o), \quad (13) \\ \hat{u}_n^o = \mu_{\theta_n}(x_{\mathcal{P}(n)}^o, x_{\mathcal{P}(n)}^e) + d_n, \quad h(x_n^e, x_n^o) \geq 0, \\ b_n = \mathcal{B}(b_{\mathcal{P}(n)}, x_n^o, x_n^e), \quad u_{\mathcal{P}(n)}^e \in \mathcal{U}^e, \\ x_{n_0}^e, x_{n_0}^o \text{ given} \quad \forall n \in \mathbb{N}_t \setminus \{n_0\}, \end{aligned}$$

where the node weight  $w_n$  represents the probability of reaching node  $n$ , which assign greater importance to nodes that are more likely to occur. At a non-root node  $n$ , the probability of a sampled  $\hat{u}_n^o$  is obtained by marginalizing over the belief state of the parent node:

$$\rho(\hat{u}_n^o | \mathcal{I}_n) = \sum_{\theta \in \Theta} b_{\mathcal{P}(n)}(\theta) \rho_\theta(\hat{u}_n^o | x_n^o, x_n^e), \quad (14)$$

where  $b_{\mathcal{P}(n)}(\theta)$  denotes the belief over  $\theta$  at the parent node, and  $\rho_\theta(\hat{u}_n^o | x_n^o, x_n^e)$  represents the likelihood of sampled action  $\hat{u}_n^o$  under the opponent policy parameterized by  $\theta$ . To normalize the sampled scenarios, the transition probability from the parent node  $\mathcal{P}(n)$  to node  $n$  is computed as

$$\Pr(n | \mathcal{P}(n)) = \frac{\rho(\hat{u}_n^o | \mathcal{I}_n)}{\sum_{i \in \mathcal{C}(\mathcal{P}(n))} \rho(u_i^o | \mathcal{I}_n)}. \quad (15)$$

The node weight is propagated recursively from the root:

$$w_n = w_{\mathcal{P}(n)} \Pr(n | \mathcal{P}(n)), \quad w_{n_0} = 1. \quad (16)$$

## 4. CONTROLLER COMPARISON AND SWITCHING STRATEGY

### 4.1 Implementation detail

In the implementation, we adopt a double integrator model to represent vehicle dynamics in Eq. (2) for simplicity. The opponent's behavior is modeled using the example in Eq. (6). To construct the scenario tree incorporating the reactive opponent model, we follow the approach of Platt et al. (2010) and implement a binary branching scheme based on  $\mu_{\text{cau}}$  and  $\mu_{\text{agg}}$ , which serve as maximum-likelihood inputs corresponding to two hypothesized values of the latent parameter  $\theta$ . The ego vehicle begins with a uniform prior belief  $b_0 = [0.5, 0.5]^\top$ . The prediction horizon and branching horizon are set to  $H = 15$  and  $H_b = 2$ , respectively, with a time step of  $\Delta t = 0.05$ . All formulations are implemented in Python using CasADi (Andersson et al., 2019) and solved using the interior-point optimizer IPOPT (Wächter and Biegler, 2006), executed on a laptop with an Intel Core i9-14900HX CPU.

### 4.2 Comparative evaluation

This comparative study primarily aims to evaluate the interactive performance of each formulation. To ensure a fair comparison across different formulations, shared parameters (e.g., objective function weights) are kept identical, while controller-specific parameters are tuned to produce similar behavior in non-interaction simulation. Additionally, fixed random seeds are used to guarantee identical initialization of simulations and opponent input samples across controllers. We evaluate controller performance through Monte Carlo simulations in the ramp merging scenario, with randomized initial positions and velocities centered around likely interaction scenarios. The results of Monte Carlo simulations are summarized in Table 2, reported as mean  $\pm$  standard deviation over 600 runs. Each MPC formulation is tested on 300 trials per opponent type (aggressive and cautious). Performance is assessed using multiple metrics: Safety is evaluated via collision rate and minimum inter-agent distance; efficiency by front-merging rate and completion time; comfort and energy by control effort (cumulative squared inputs) and maximal absolute acceleration; and overall performance by trajectory cost, defined as the accumulated stage cost  $l$  over the trajectory.

In Table 2, robust MPC yields the largest minimum distance, longest completion time, and highest control effort, indicating strong safety guarantees at the expense of conservative and less comfortable behavior. In contrast, non-reactive branch MPC reduces completion time while

Table 2. Monte Carlo simulations in the ramp-merging scenario

Metric	Robust	Non-reactive branch	Reactive branch	Explicit dual	Implicit dual	Switching
Safety rate (%)	100.0	100.0	100.0	100.0	100.0	100.0
Min distance (m)	$4.13 \pm 0.29$	$1.99 \pm 0.30$	$2.67 \pm 0.27$	$3.11 \pm 0.25$	$3.02 \pm 0.27$	$3.24 \pm 0.35$
Front-merging rate (%)	1.0	4.6	24.6	47.3	43.0	44.8
Completion time (s)	$5.85 \pm 0.48$	$5.22 \pm 0.42$	$4.93 \pm 0.37$	$4.62 \pm 0.32$	$4.65 \pm 0.37$	$4.67 \pm 0.21$
Max abs. acc. (m/s <sup>2</sup> )	$3.39 \pm 0.41$	$2.21 \pm 0.56$	$1.02 \pm 0.45$	$1.52 \pm 0.53$	$0.93 \pm 0.42$	$0.88 \pm 0.47$
Control effort	$105.3 \pm 7.8$	$54.1 \pm 7.3$	$16.2 \pm 4.5$	$22.9 \pm 5.9$	$12.6 \pm 3.7$	$14.5 \pm 6.1$
Trajectory cost (lower is better)	$578.8 \pm 42.6$	$314.8 \pm 45.7$	$109.7 \pm 29.1$	$80.6 \pm 23.5$	$68.9 \pm 22.3$	$72.3 \pm 19.8$
Averaged Computation time (s)	$0.047 \pm 0.005$	$0.324 \pm 0.020$	$0.431 \pm 0.115$	$0.434 \pm 0.116$	$1.148 \pm 0.148$	$0.313 \pm 0.279$

enhancing comfort and save energy. Incorporating opponent reactions significantly increases the front-merging rate. Compared to both branch MPC variants, the two dual MPC variants achieve shorter completion times while preserving a larger minimum distance, reflecting simultaneous improvements in safety and efficiency attributable to increased front-merging behavior. Compared to the explicit approach that may initiate active probing even when unnecessary, the implicit approach achieves the lowest trajectory cost and superior overall performance by triggering probing only when deemed beneficial.

The front-merging rate serves as a proxy for decision-level efficiency, which is critical for improving efficiency without compromising safety. The incremental integration of scenario trees, opponent reaction modeling, and belief updates progressively increases this rate, highlighting their positive contribution to interaction-aware decision-making. Consequently, the more advanced the interaction modeling, the better the interactive performance. Thus, interactive capability can be hierarchized based on the underlying level of interaction modeling.

#### 4.3 Switching interactive MPCs as needed

Table 2 shows that higher levels of interactive controller lead to increased computational time. Specifically, the computational burden of the implicit dual MPC is over 20 times greater than that of the robust MPC. Dual MPC is computationally intensive, especially in realistic traffic scenarios with multiple vehicles and complex environment. Although more powerful hardware or efficient algorithms can help accelerate computation, deploying dual MPC in all situations would consume limited and valuable onboard computational resources and energy. However, the majority of driving does not involve strong interaction with other agents. Given this, it is essential to adaptively select the appropriate level of interactive controller based on the real-time situation.

#### Algorithm 1 Situation-Aware Switching Controller

**Input:** Ego state  $x_t^e$ , opponent state  $x_t^o$ , belief state  $b_t$

- 1: Construct feature vector:  $z_t \leftarrow [(x_t^e)^\top, (x_t^o)^\top, b_t^\top]^\top$
- 2: Predict controller probabilities:  $\pi_t \leftarrow \mathbf{NN}(z_t)$
- 3: Select controller index:  $i^* \leftarrow \arg \max_{i \in \{1, \dots, m\}} \pi_t[i]$
- 4: Compute control inputs:  $\mathbf{U}_t^e \leftarrow \mathbf{MPC}_{i^*}(x_t^e, x_t^o, b_t)$
- 5: Extract the first control input:  $u_t^e \leftarrow \mathbf{U}_t^e[1]$
- 6: **return**  $u_t^e$

We consider a set of MPC controllers with varying levels of interaction awareness, denoted by  $\mathcal{MPC} =$

$\{\mathbf{MPC}_1, \dots, \mathbf{MPC}_m\}$ . To enable situation-aware selection among them, we design a fully connected neural network  $\mathbf{NN} : \mathbb{R}^d \rightarrow \mathbb{R}^m$ . The network takes as input a feature vector representing the traffic scenario, defined as  $z_t = [(x_t^e)^\top, (x_t^o)^\top, b_t^\top]^\top \in \mathbb{R}^d$ , which concatenates the ego state  $x_t^e$ , opponent state  $x_t^o$ , and belief state  $b_t$ . The network output is a probability vector  $\pi_t = \mathbf{NN}(z_t)$ , where  $\pi_t[i]$  denotes the probability assigned to controller  $\mathbf{MPC}_i$ . The protocol of the switching controller is provided in Alg. 1.

To construct the training dataset, we simulate over 10,000 randomly generated traffic scenarios. For each scenario with feature vector  $z$ , we evaluate controllers using the following composite performance metric:

$$J(\mathbf{MPC}_i; z) = J_{\text{traj}}(\mathbf{MPC}_i; z) - \beta \cdot \mathbf{1}_{\text{front}}(\mathbf{MPC}_i; z),$$

where  $J_{\text{traj}}(\mathbf{MPC}_i; z)$  is the cumulative trajectory cost over the predictive horizon,  $\beta > 0$  is a reward weight, and  $\mathbf{1}_{\text{front}}(\mathbf{MPC}_i; z)$  is an indicator function equal to 1 if controller  $\mathbf{MPC}_i$  selects a front-merge maneuver in scenario  $z$ , and 0 otherwise. Let  $J^*(z) = \min_i J(\mathbf{MPC}_i; z)$  denote the best achievable cost in scenario  $z$ . A controller  $\mathbf{MPC}_i$  is considered *near-optimal* if  $J(\mathbf{MPC}_i; z) \leq J^*(z) + \epsilon$ , where  $\epsilon > 0$  is a tolerance threshold. Each scenario is labeled with a one-hot vector  $\pi^*(z)$ , where only one entry is set to 1 and the rest to 0. The selected controller index is defined as  $i^*(z) = \min \{i \mid J(\mathbf{MPC}_i; z) \leq J^*(z) + \epsilon\}$ , and the corresponding label is given by  $\pi^*[i] = \mathbf{1}(i = i^*(z))$ , favoring the lowest-level controller that achieves near-optimal performance.

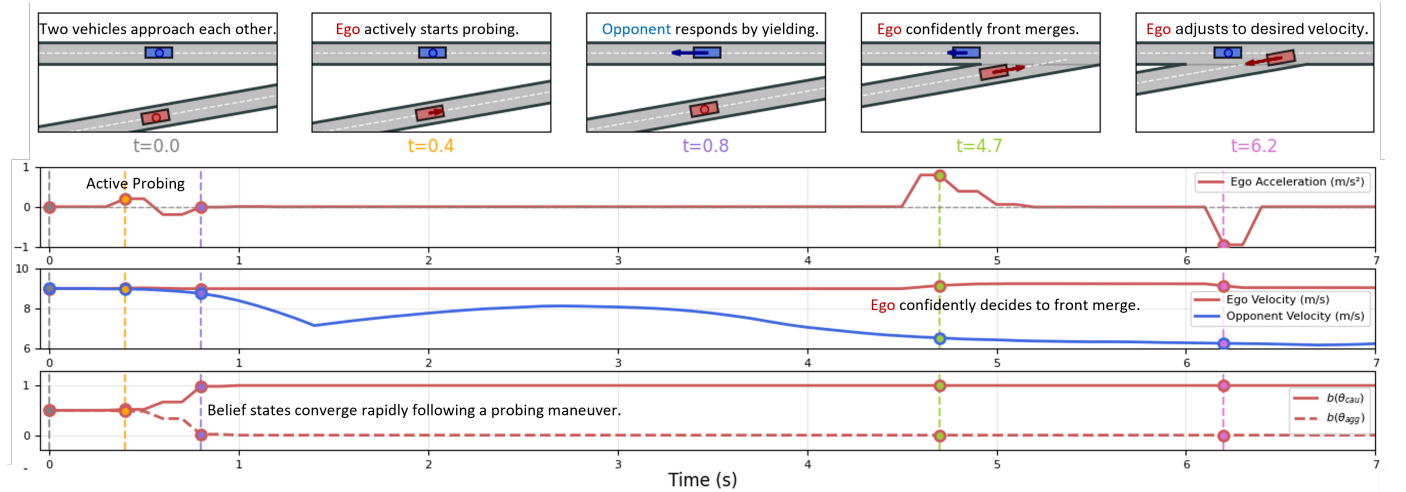
Given that higher-level MPCs exhibit superior interactive behavior, mistakenly selecting lower-level controllers can degrade interaction performance. Thus, we design a loss function to encourage the classifier to select higher-level controllers by penalizing incorrect choices of lower-level controllers more heavily than those of higher-level ones. Let  $\pi_t = \mathbf{NN}(z_t)$  denote the predicted distribution over controllers and  $\pi^*(z)$  the ground-truth label. The loss is defined as  $\mathcal{L}(z) = \sum_{i=1}^3 w(i, i^*(z)) \cdot (-\pi_i^*(z) \log \pi_i)$ , where  $w(i, i^*)$  is a weighting function satisfying

$$w(i, i^*) = \begin{cases} \alpha^{i^* - i}, & \text{if } i < i^*, \\ 1, & \text{otherwise,} \end{cases}$$

and  $\alpha > 1$  is a tunable penalty factor that increases the cost of selecting a lower-level controller.

#### 5. EVALUATION OF SWITCHING CONTROLLER

In the implementation, we select robust MPC, reactive branch MPC, and implicit dual MPC as candidate controllers. The neural network consists of three hidden layers



(a) Simulation of the implicit dual MPC interacting with a cautious opponent. The ego vehicle’s desired velocity is set to 9 m/s. In the snapshots, the arrows on the vehicles represent their acceleration vectors.



(b) Control inputs (accelerations) produced by the switching controller. The colored regions indicate which policy is active: blue for the implicit dual MPC, green for the reactive branch, and red for the robust MPC.

Fig. 3. Simulation of an interactive scenario that reveals active information-seeking (probing) behavior.

with 128, 64, and 32 neurons, respectively. The trained neural network classifier achieves a test accuracy of 94.5%. And then, we evaluate the switching controller within the same Monte Carlo simulation framework. The results, summarized in Table 2, show that the switching controller maintains performance comparable to that of the implicit dual MPC. Notably, the average computational time is reduced by nearly a factor of three. Across all Monte Carlo simulation steps, only 1.4% of steps necessitate the implicit dual MPC, while 42.3% are handled by reactive branching MPC, and 56.3% by robust MPC. This highlights a key result: Employing high-level interactive controllers in only a small subset of critical situations can lead to substantial performance improvements. This finding underscores the effectiveness of the switching strategy, which is further illustrated through the following specific scenarios.

### 5.1 Ramp merging

We select one representative scenario of ramp merging in which the dual MPC chooses a front-merging strategy, whereas other formulations opt for a back-merge. The entire process is illustrated in Fig. 3a. The acceleration profile reveals an active probing maneuver executed by the dual MPC at  $t = 0.6s$ . Specifically, the dual MPC applies a short-time acceleration to elicit a response from the opponent vehicle. Upon observing a yielding reaction, the belief state rapidly converges, indicating a high likelihood that the driving style of the opponent is cautious. As a result, the ego vehicle confidently proceeds with the front-merge maneuver and maintains its desired speed, as shown in the velocity profiles. In contrast, the other approaches lack information-seeking behavior and default to a back-merge strategy due to parametric uncertainty.

This scenario clearly demonstrates the active probing behavior of the implicit dual MPC and highlights its benefits. We now examine whether the switching controller can inherit this advantage. To this end, we simulate the same scenario using the switching controller, which is also able to achieve a front-merge maneuver. The control inputs generated over time are shown in Fig. 3b. Notably, the implicit dual MPC is employed for only 8.6% of the process, specifically when active probing is required. Once the belief state has converged, the switching controller transitions to a reactive branching strategy to maintain the desired speed prior to the merging point. As the ego vehicle approaches the merge location with a slight positional advantage for a front-merge, the controller switches to a robust MPC to ensure safety. This simulation demonstrates that the switching controller effectively replicates the active information-seeking behavior of the dual MPC.

### 5.2 Unsignalized intersection

In Fig. 4, we evaluate the proposed method in an unsignalized intersection scenario. Similar to the ramp-merging case, the dual MPC is selected to trigger active probing behavior, while the robust MPC is employed to ensure safety as the vehicles approach each other. In Monte Carlo simulations with random initialization, the proposed switching controller achieves a 46.2% first-crossing rate, comparable to the 48.5% of the implicit dual MPC and substantially higher than the 23.9% of the reactive branch MPC and the 2.6% of the robust MPC. Notably, its total computation time is reduced by 79.3% relative to the implicit dual MPC and by 42.6% to the reactive branch MPC. This results demonstrate the scalability of the proposed approach to general interactive scenarios.

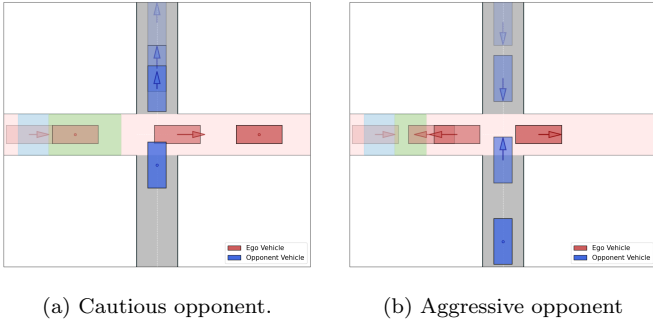


Fig. 4. Interaction with an opponent in an unsignalized intersection. The colored regions indicate which policy is active: blue for the implicit dual MPC, green for the reactive branch, and red for the robust MPC.

## 6. CONCLUSION

This paper presents clear formulations of representative MPC controllers recently proposed for handling interactive scenarios and conducts a fair comparison to highlight their levels of interaction and distinct behavioral characteristics, offering insights into complex interactions and clarifying differences across varying interactive controllers. Building on these insights, we design a neural network-based classifier that selects the most appropriate controller based on real-time situational demands. Extensive simulations in two typical traffic scenarios demonstrate that invoking the most advanced interactive controller only in rare but critical situations can markedly improve overall performance while greatly reducing the computational burden.

## REFERENCES

Andersson, J.A.E., Gillis, J., Horn, G., Rawlings, J.B., and Diehl, M. (2019). CasADi – A software framework for nonlinear optimization and optimal control. *Mathematical Programming Computation*, 11(1), 1–36.

Arcari, E., Hewing, L., and Zeilinger, M.N. (2020). An approximate dynamic programming approach for dual stochastic model predictive control. *IFAC-PapersOnLine*, 53(2), 8105–8111.

Baltussen, T.M., Lefever, A.E., Tóth, R., Heemels, W., and Katriniok, A. (2025). Online learning of interaction dynamics with dual model predictive control for multi-agent systems using gaussian processes. In *American Control Conference*.

Batkovic, I., Rosolia, U., Zanon, M., and Falcone, P. (2021). A robust scenario mpc approach for uncertain multi-modal obstacles. *IEEE Control Systems Letters*, 5(3), 947–952.

Cesari, G., Schildbach, G., Carvalho, A., and Borrelli, F. (2017). Scenario model predictive control for lane change assistance and autonomous driving on highways. *IEEE Intelligent Transportation Systems Magazine*, 9(3), 23–35.

Chen, Y., Rosolia, U., Ubellacker, W., Csomay-Shanklin, N., and Ames, A.D. (2022). Interactive multi-modal motion planning with branch model predictive control. *IEEE Robotics and Automation Letters*, 7(2), 5365–5372.

Hu, H., Isele, D., Bae, S., and Fisac, J.F. (2024). Active uncertainty reduction for safe and efficient interaction planning: A shielding-aware dual control approach. *The International Journal of Robotics Research*, 43(9), 1382–1408.

Knaup, J., D’sa, J., Chalaki, B., Naes, T., Mahjoub, H.N., Moradi-Pari, E., and Tsotras, P. (2024). Active learning with dual model predictive path-integral control for interaction-aware autonomous highway on-ramp merging. In *2024 IEEE International Conference on Robotics and Automation (ICRA)*, 14191–14197. IEEE.

Langson, W., Chryssochoos, I., Raković, S., and Mayne, D.Q. (2004). Robust model predictive control using tubes. *Automatica*, 40(1), 125–133.

Mesbah, A. (2018). Stochastic model predictive control with active uncertainty learning: A survey on dual control. *Annual Reviews in Control*, 45, 107–117.

Muraleedharan, A., Tran, A.T., Okuda, H., and Suzuki, T. (2020). Scenario-based model predictive speed controller considering probabilistic constraint for driving scene with pedestrian. In *2020 IEEE 23rd International Conference on Intelligent Transportation Systems (ITSC)*.

Oliveira, R., Nair, S.H., and Wahlberg, B. (2023). Interaction and decision making-aware motion planning using branch model predictive control. In *2023 IEEE Intelligent Vehicles Symposium (IV)*, 1–8. IEEE.

Platt, R., Tedrake, R., Kaelbling, L., and Lozano-Perez, T. (2010). Belief space planning assuming maximum likelihood observations. In *Proceedings of Robotics: Science and Systems*. Zaragoza, Spain.

Sadigh, D., Landolfi, N., Sastry, S.S., Seshia, S.A., and Dragan, A.D. (2018). Planning for cars that coordinate with people: leveraging effects on human actions for planning and active information gathering over human internal state. *Autonomous Robots*, 42, 1405–1426.

Scokaert, P. and Mayne, D. (1998). Min-max feedback model predictive control for constrained linear systems. *IEEE Transactions on Automatic Control*, 43(8), 1136–1142.

Tian, R., Sun, L., Tomizuka, M., and Isele, D. (2021). Anytime game-theoretic planning with active reasoning about humans’ latent states for human-centered robots. In *2021 IEEE International Conference on Robotics and Automation (ICRA)*, 4509–4515. IEEE.

Wächter, A. and Biegler, L.T. (2006). On the implementation of an interior-point filter line-search algorithm for large-scale nonlinear programming. *Mathematical programming*, 106, 25–57.

Wang, W., Wang, L., Zhang, C., Liu, C., and Sun, L. (2022). Social interactions for autonomous driving: A review and perspectives. *Foundations and Trends® in Robotics*, 10(3–4), 198–376.

Wang, W., Xi, J., and Hedrick, J.K. (2019). A learning-based personalized driver model using bounded generalized gaussian mixture models. *IEEE Transactions on Vehicular Technology*, 68(12), 11679–11690.

Zanardi, A., Bolognani, S., Censi, A., and Frazzoli, E. (2021). Game theoretical motion planning. *IEEE International Conference on Robotics and Automation (ICRA)*, Tutorial.

Zhou, J., Tian, D., Sheng, Z., Duan, X., Qu, G., Zhao, D., Cao, D., and Shen, X. (2022). Robust min-max model predictive vehicle platooning with causal disturbance feedback. *IEEE Transactions on Intelligent Transportation Systems*, 23(9), 15878–15897.